



Revealing the Progenitor of SN 2021zby through Analysis of the TESS Shock-cooling Light Curve

Qinan Wang¹ , Patrick Armstrong² , Yossef Zenati^{1,29,30} , Ryan Ridden-Harper³ , Armin Rest^{1,4} , Iair Arcavi^{5,6} , Charles D. Kilpatrick⁷ , Ryan J. Foley⁸ , Brad E. Tucker^{2,9,10} , Chris Lidman^{11,12} , Thomas L. Killestein¹³ , Melissa Shahbandeh¹ , Joseph P Anderson^{14,15} , Rodrigo Angulo¹ , Chris Ashall¹⁶ , Jamison Burke^{17,18} , Ting-Wan Chen¹⁹ , Sophie von Coelln¹ , Kyle A. Dalrymple¹ , Kyle W. Davis⁸ , Michael D. Fulton²⁰ , Lluís Galbany^{21,22} , Estefania Padilla Gonzalez^{17,18} , Bore Gao¹ , Mariusz Gromadzki²³ , D. Andrew Howell^{17,18} , Nada Ihanec^{14,23} , Jacob E. Jencson¹ , David O. Jones²⁴ , Joseph D. Lyman¹³ , Curtis McCully¹⁷ , Tomás E. Müller-Bravo^{21,22} , Megan Newsome^{17,18} , Matt Nicholl²⁵ , David O'Neill¹³ , Craig Pellegrino^{17,18} , Sofia Rest²⁶ , Stephen J. Smartt^{20,27} , Ken Smith²⁰ , Shubham Srivastav²⁰ , Giacomo Terreran^{17,18} , Samaporn Tinyanont⁸ , David R. Young²⁰ , and Alfredo Zenteno²⁸

¹ Physics and Astronomy Department, Johns Hopkins University, Baltimore, MD 21218, USA; qwang75@jhu.edu

² Mt Stromlo Observatory, The Research School of Astronomy and Astrophysics, Australian National University, Weston Creek, ACT 2601, Australia

³ School of Physical and Chemical Sciences | Te Kura Matū, University of Canterbury, Private Bag 4800, Christchurch 8140, New Zealand

⁴ Space Telescope Science Institute, Baltimore, MD 21218, USA

⁵ The School of Physics and Astronomy, Tel Aviv University, Tel Aviv 69978, Israel

⁶ CIFAR Azrieli Global Scholars program, CIFAR, Toronto, Canada

⁷ Center for Interdisciplinary Exploration and Research in Astrophysics (CIERA), Northwestern University, Evanston, IL 60208, USA

⁸ Department of Astronomy and Astrophysics, University of California, Santa Cruz, CA 95064, USA

⁹ National Centre for the Public Awareness of Science, Australian National University, Canberra, ACT 2611, Australia

¹⁰ The ARC Centre of Excellence for All-Sky Astrophysics in 3 Dimension (ASTRO 3D), Australia

¹¹ Centre for Gravitational Astrophysics, College of Science, The Australian National University, Acton, ACT 2601, Australia

¹² The Research School of Astronomy and Astrophysics, Australian National University, Stromlo, ACT 2601, Australia

¹³ Department of Physics, University of Warwick, Gibbet Hill Road, Coventry CV4 7AL, UK

¹⁴ European Southern Observatory, Alonso de Córdova 3107, Casilla 19, Santiago, Chile

¹⁵ Millennium Institute of Astrophysics MAS, Nuncio Monsenor Sotero Sanz 100, Off. 104, Providencia, Santiago, Chile

¹⁶ Department of Physics, Virginia Tech, 850 West Campus Drive, Blacksburg, VA, 24061, USA

¹⁷ Las Cumbres Observatory, 6740 Cortona Drive, Suite 102, Goleta, CA 93117-5575, USA

¹⁸ Department of Physics, University of California, Santa Barbara, CA 93106-9530, USA

¹⁹ The Oskar Klein Centre, Department of Astronomy, Stockholm University, AlbaNova, SE-10691 Stockholm, Sweden

²⁰ Astrophysics Research Centre, School of Mathematics and Physics, Queen's University Belfast, Belfast BT7 1NN, UK

²¹ Institute of Space Sciences (ICE, CSIC), Campus UAB, Carrer de Can Magrans, s/n, E-08193 Barcelona, Spain

²² Institut d'Estudis Espacials de Catalunya (IEEC), E-08034 Barcelona, Spain

²³ Astronomical Observatory, University of Warsaw, Al. Ujazdowskie 4, 00-478 Warszawa, Poland

²⁴ Gemini Observatory, NSF's NOIRLab, 670 N. A'ohoku Place, Hilo, HI 96720, USA

²⁵ Birmingham Institute for Gravitational Wave Astronomy and School of Physics and Astronomy, University of Birmingham, Birmingham B15 2TT, UK

²⁶ Department of Computer Science, Johns Hopkins University, Baltimore, MD 21218, USA

²⁷ Department of Physics, University of Oxford, Oxford, OX1 3RH, UK

²⁸ Cerro Tololo Inter-American Observatory, NSF's NOIRLab, Casilla 603, La Serena, Chile

Received 2022 November 6; revised 2023 January 2; accepted 2023 January 3; published 2023 January 31

Abstract

We present early observations and analysis of the double-peaked Type IIb supernova (SN IIb) SN 2021zby. TESS captured the prominent early shock-cooling peak of SN 2021zby within the first ~ 10 days after explosion with a 30 minute cadence. We present optical and near-infrared spectral series of SN 2021zby, including three spectra during the shock-cooling phase. Using a multiband model fit, we find that the inferred properties of its progenitor are consistent with a red supergiant or yellow supergiant, with an envelope mass of $\sim 0.30\text{--}0.65 M_{\odot}$ and an envelope radius of $\sim 120\text{--}300 R_{\odot}$. These inferred progenitor properties are similar to those of other SNe IIb with a double-peaked feature, such as SNe 1993J, 2011dh, 2016gkg, and 2017jgh. This study further validates the importance of the high cadence and early coverage in resolving the shape of the shock-cooling light curve, while the multiband observations, particularly UV, are also necessary to fully constrain the progenitor properties.

Unified Astronomy Thesaurus concepts: Core-collapse supernovae (304); Supernovae (1668)

Supporting material: data behind figures

1. Introduction

Type IIb supernovae (SNe IIb) are characterized by the presence of hydrogen lines at early phases typical of Type II supernovae (SNe II), which fade at later phases as helium features begin to dominate the spectra (Filippenko et al. 1993). In the weeks following the explosion, the spectra of the supernovae will therefore transition from Type II to Type I.

²⁹ CHE Israel Excellence Fellowship.

³⁰ ISEF Fellowship.

This evolution can be explained by the progenitor star losing most, but not all, of its hydrogen-rich envelope before explosion. The exact progenitors of SNe I Ib are currently not fully understood with two leading possibilities (Ensmann & Woosley 1988; Woosley et al. 1993; Heger et al. 2003; Dessart et al. 2011; Smith 2017; Sravan et al. 2020; Long et al. 2022): (1) a low-mass star ($<20 M_{\odot}$) in a binary system or (2) an isolated high-mass star (25–80 M_{\odot}).

The transition from hydrogen-rich progenitors to stripped-envelope progenitors is not fully understood, neither is the exact mass of hydrogen (Gilkis & Arcavi 2022) as two evolutionary pathways are possible and each scenario involves different masses and nuclear burning instabilities (Arnett & Meakin 2011; Arnett et al. 2018). In the low-mass binary case, mass loss occurs through binary interactions when one of the stars enters its red giant phase (Sana et al. 2012; Soker 2017; Yoon et al. 2017; Gilkis et al. 2019; Lohev et al. 2019). In the second case of a high-mass star, mass loss is believed to be as a result of strong stellar winds. In a few cases, the progenitors of SNe I Ib have been directly identified in pre-SN images as supergiants with radii $\gtrsim 200R_{\odot}$, such as SN 1993J (Aldering et al. 1994; Maund et al. 2004), SN 2011dh (Arcavi et al. 2011; Maund et al. 2011; Bersten et al. 2012; Van Dyk et al. 2013; Folatelli et al. 2014), and SN 2013df (Van Dyk et al. 2014).

In some rare cases, massive stars may lose their hydrogen-rich envelope of a few solar masses and explode as SNe I Ib with a prominent early flux excess that precedes the main radioactive peak (e.g., Arcavi et al. 2011; Sana et al. 2012; Gal-Yam 2017; Fang et al. 2022). The prominent early peak in the optical light curve can last for a few days after explosion. This peak is believed to come from the cooling of shock-heated ejecta after shock breakout and is thus called a shock-cooling light curve (SCL; Gal-Yam 2017). These double-peaked phenomena have been discovered and analyzed in a few cases such as SN 1993J (Matheson et al. 2000; Maund et al. 2004), SN 2011dh (Arcavi et al. 2011; Ergon et al. 2015), SN 2016gkg (Arcavi et al. 2017a), and SN 2017jgh (Armstrong et al. 2021) etc. SNe I Ib are also core-collapse SNe that are on occasion double-peaked. They are stripped off their hydrogen and helium layers and identified by no H/He lines and weak silicon features in their optical spectra (Filippenko & Sargent 1985; Clocchiatti et al. 1996; Woosley et al. 2002; Smith et al. 2008; Drout et al. 2011; Prentice et al. 2016; Dessart et al. 2021; Karamahmetoglu et al. 2022). Candidate progenitors have been identified in images for two SNe I Ib, iPTF13bvn and SN 2019yvr (Cao et al. 2013; Kilpatrick et al. 2021; Gilkis & Arcavi 2022). For other multi-peaked SNe see Foley et al. (2007), Arcavi et al. (2017b), Gomez et al. (2021), Zenati et al. (2022), and Chen et al. (2022).

Continuous, high-cadence monitoring of the early light curve is key to capturing and analyzing the complete SCL. High-cadence imaging from space telescopes such as the Kepler Space Telescope (Kepler; Haas et al. 2010; Howell et al. 2014) and the Transiting Exoplanet Survey Satellite (TESS; Ricker et al. 2014) are ideal to monitor such short-timescale transient phenomena. Observations from these telescopes have enabled some ground-breaking discoveries on the progenitors of various SNe (e.g., Dimitriadis et al. 2019; Fausnaugh et al. 2021; Vallely et al. 2019; Wang et al. 2021; Pearson et al. 2022; Andrews et al. 2022). In particular, Armstrong et al. 2021 analyzed the SCL of the Type I Ib SN 2017jgh that was fully covered by Kepler/K2. With the high-cadence coverage

of the complete SCL, the progenitor properties were estimated with high precision. Armstrong et al. (2021) further demonstrate that without the high-cadence Kepler/K2 light curve during the rise, the fitting results would exhibit a systematic offset, and the estimations for the envelope radius, offset time, and ejecta velocity can be biased by $\sim 15\%$, 20% , and 25% , respectively, for this specific event.

Here we present the evolution of SN 2021zby during the first ~ 2 months after explosion with a spectrophotometric time series in the optical and near-infrared (NIR). SN 2021zby was discovered by the Asteroid Terrestrial-impact Last Alert System (ATLAS; Tonry et al. 2018; Smith et al. 2020) on 2021 September 17 10:52:19.200 UTC, Modified Julian Date (MJD) 59,474.45, in the o band with $m_o = 18.16 \pm 0.14$ (Smith et al. 2021) and was spectroscopically classified as an SN I Ib (Hinkle 2021; Fulton et al. 2021).

SN 2021zby is located in a spiral arm of NGC 1166 at coordinates $\alpha = 03^{\text{h}}00^{\text{m}}35^{\text{s}}.63$, $\delta = +11^{\circ}50'29'' 74$ (J2000.0). Prior to SN 2021zby, two other transients, the unclassified PS1-14abm (Huber et al. 2015) and SN II 2018htf (Berton et al. 2018; Gagliano et al. 2018), had been discovered in NGC 1166 in the past 10 years. Both of them are at least $3''$ away and are not associated with SN 2021zby. We adopt a redshift of $z = 0.025965 \pm 0.00002$ from HI 21 cm measurements (Springob et al. 2005) and a distance of 106.1 Mpc, corresponding to a distance modulus of ~ 35.12 mag. The Milky Way extinction is relatively high toward this direction, with $E(B - V)_{\text{MW}} = 0.21$ (Schlafly & Finkbeiner 2011). The early TESS light curve of SN 2021zby starts at MJD 59,473.8 and ends at MJD 59,498.4, shortly before the time of the main radioactive peak. Combined with the i - and o -band measurements from the Dark Energy Camera (DECam; Flaugher et al. 2015) and ATLAS with similar effective wavelengths around a similar phase, we can infer the radioactive peak to be at $t_{\text{max}} = 59499 \pm 1$ MJD in the TESS band.

TESS coverage of SN 2021zby started shortly before explosion with ~ 12 hr of nondetection with a magnitude limit $m_{\text{TESS}} \gtrsim 19.38$ at the beginning of sector 43. As inferred from the SCL fitting discussed in Section 3.1, the time of explosion t_0 is around MJD $\sim 59,474.4 \pm 0.1$, ~ 24 days prior to t_{max} . There was no clear detection of a short-duration shock breakout flash in the TESS light curve around the time of explosion. Systematic noise from scattered light and relatively low luminosity in redder bands (Nakar & Sari 2010) like TESS may limit the detectability of the shock breakout flash in this case. Throughout this Letter, phases are presented relative to the inferred time of explosion t_0 , except for the model-fitting section where t_0 is a free parameter to be constrained.

Throughout this Letter, observed times are reported in MJDs while phases, unless noted otherwise, are reported in the rest frame. We adopt the AB magnitude system, unless noted otherwise, and a flat Λ CDM cosmological model with $H_0 = 73 \text{ km s}^{-1} \text{ Mpc}^{-1}$ (Riess et al. 2016, 2018). All the data presented in this paper will be made public via WISEREP³¹ (Yaron & Gal-Yam 2012).

2. Observations and Data Reduction

ATLAS observed SN 2021zby throughout the preexplosion and double-peaked stage in the o band, and also in the postpeak stage in both o and c bands. We also obtained ground-based

³¹ <https://www.wiserep.org/object/19385>

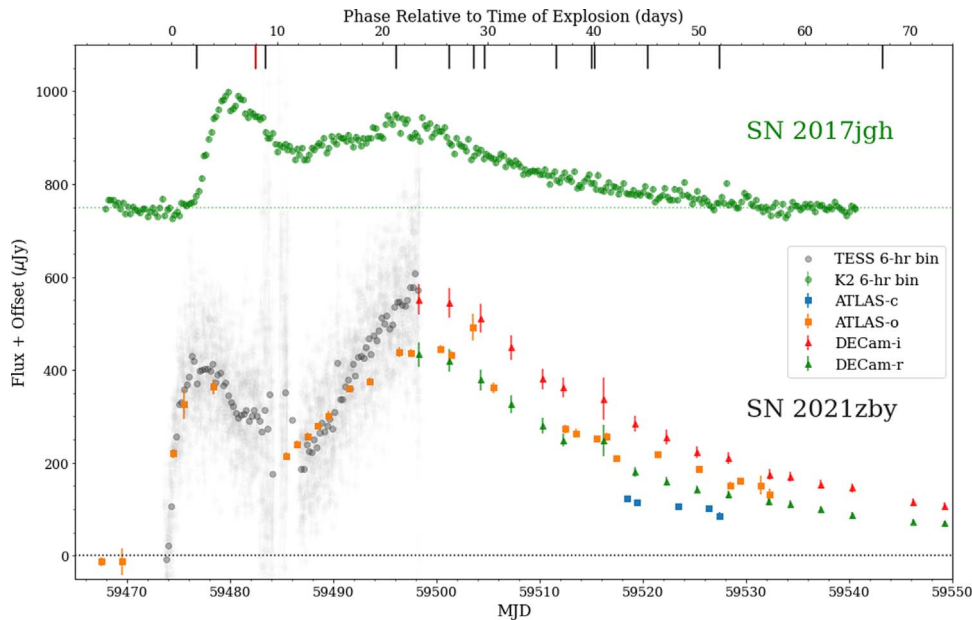


Figure 1. Optical light curves of SN 2021zby from TESS and ground-based surveys in comparison with the Kepler light curve of SN 2017jgh (Armstrong et al. 2021). Black ticks at the top of the plot mark the times where ground-based optical spectra were obtained for SN 2021zby; red tick marks represent the NIR spectrum taken by IRTF. Notice that the TESS Sector 43 started ~ 12 hr before the time of explosion and thus there’s only one nondetection in the binned light curve in the preexplosion phase.

(The data used to create this figure are available.)

photometric follow-up in the postpeak stage with DECam on the Cerro Tololo Inter-American Observatory (CTIO) 4-m Blanco telescope (DePoy et al. 2008; Flaughner et al. 2015) in the r and i bands. Multiband light curves are plotted in Figure 1, in comparison with the Kepler light curve of SN 2017jgh. In addition, we obtained spectra from multiple ground-based observatories. Details of these spectra are listed in the Appendix.

To measure significant SN flux detection at the location of SN 2021zby, we applied several cuts on the total number of individual as well as averaged data in order to identify and remove bad measurements. Our first cut used the chi-square and uncertainty values of the point-spread function (PSF) fitting to clean out bad data. We then obtained forced photometry of eight control light curves located in a circular pattern around the location of the SN with a radius of $17''$. The flux of these control light curves is expected to be consistent with zero within the uncertainties, and any deviation from that would indicate that there are either unaccounted systematics or underestimated uncertainties. We searched for such deviations by calculating the 3σ -clipped average of the set of control light-curve measurements for a given epoch (for a more detailed discussion see S. Rest et al. 2023, in preparation). This mean of the photometric measurements is expected to be consistent with zero and, if not, we flag and remove those epochs from the SN light curve. We then binned the SN 2021zby light curve by calculating a 3σ -clipped average for each night, excluding the flagged measurements from the previous step. This method has been applied in a few other studies and proven its reliability in successfully removing bad measurements from the SN light curve (e.g., Jacobson-Galán et al. 2022).

Following standard calibrations (bias correction, flat-fielding, and World Coordinate System (WCS)) using the NSF NOIRLab DECam Community Pipeline (Valdes et al. 2014),

we reduced the DECam data using the `Photpipe` pipeline as described in Rest et al. (2005, 2014). The images were warped into a tangent plane of the sky using the `swarp` routine (Bertin et al. 2002), after which photometry of the stellar sources was obtained using the standard PSF-fitting software `DoPHOT` (Schechter et al. 1993). We then used the PS1 catalog (Flewelling et al. 2020) converted into the DECam natural system as described in Scolnic et al. (2015) to obtain the photometric zero-points. The images were then kernel- and flux-matched to template images, subtracted, and masked using the `hotpants` code (Becker 2015), which is based on the Alard–Lupton algorithm (Alard & Lupton 1998). The 3σ -clipped average position of SN 2021zby was calculated from all of the significant detections in the difference images to within $0.75''$ of the reported position. The final light curves were then obtained by performing forced photometry on this position for all images. The r - and i -band template images were taken after SN 2021zby was discovered, and therefore contain some residual SN flux. Thus, for each of these filters, we adjusted the light curves by adding a common flux offset so that the magnitudes match the ATLAS light curves, using an approximate conversion from Tonry et al. (2018):

$$r \sim 0.35 c + 0.65 o, i \sim -0.39 c + 1.39 o. \quad (1)$$

TESS observed SN 2021zby in full-frame images (FFIs) for sectors 42, 43, and 44 (hereafter S42, S43, and S44), at a 10 minute cadence.³² These three sectors covered preexplosion (S42), double-peaked rise (S43), and decline (S44), which gives excellent coverage of the event outside of the 1 day mid-sector and inter-sector gaps. We reduced all sectors of TESS data using the `TESSreduce` python package, which aligns images, subtracts the variable background, and provides a flux

³² The original calibrated TESS FFIs can be found in the the Mikulski Archive for Space Telescopes (MAST): doi:10.17909/0cp4-2j79.

calibration from field stars (Ridden-Harper et al. 2021). One alteration was made to the default `TESSreduce` reduction where we included the nearby bad column 1167 in S43 data into the automatically determined strap mask. This inclusion rescaled the column producing a clean background subtraction for the nearby pixels that were used in the 3×3 aperture for SN 2021zby. Since `TESSreduce` produced difference-imaged light curves, we must add an offset to the light curves for S43 and S44 as the flux from SN 2021zby was included in the reference images. We estimated the offsets by calculating synthetic photometry in the TESS bandpass from spectra and photometry in other bands that were covered by TESS observations. Since the spectra do not cover the full TESS wavelength range 5802.57–11171.45 Å, we extrapolated the spectra by assuming blackbody emission with temperature $\sim 83,000$ K estimated from the optical spectrum³³ when calculating synthetic photometry. During S43 scattered light from the Earth and Moon in the detector reached saturation, making the photometry unreliable from MJD 59,499 to 59,524. The reduced TESS light curve was further binned with 6 hr bin to improve the signal-to-noise ratio (S/N), as shown in Figure 1.

We obtained optical spectra with instruments including the Wide-Field Spectrograph (WiFeS; Dopita et al. 2007) on the 2.3 m telescope at Siding Spring Observatory (SSO), the IDS long-slit spectrograph on the 2.5 m Isaac Newton Telescope (INT), the Kast spectrograph on the 3 m Shane Telescope at Lick Observatory, the ESO Faint Object Spectrograph and Camera (EFOSC2; Buzzoni et al. 1984) on the ESO New Technology Telescope (NTT, as part of the ePESSTO+ survey; Smartt et al. 2015), the Spectrograph for the Rapid Acquisition of Transients (SPRAT; Piascik et al. 2014) on the Liverpool Telescope, and the Las Cumbres Observatory FLOYDS spectrographs mounted on the 2-meter Faulkes Telescope North (FTN) and South (FTS) at Haleakala Observatory and SSO, respectively, through the Global Supernova Project.

The IDS spectrum was reduced and flux-calibrated appropriately using the standard the Image Reduction and Analysis Facility (IRAF; Tody 1986) `specred` routines. The EFOSC2 spectra were reduced in a similar manner, with the aid of the PESSTO pipeline.³⁴ The KAST spectra were reduced using a custom data reduction pipeline based on IRAF.³⁵ One-dimensional FLOYDS spectra from FTN and FTS were extracted, and flux and wavelength calibrated using the `floyds_pipeline`³⁶ (Valenti et al. 2013). The WiFeS data were processed with the PyWiFeS pipeline³⁷ (Childress et al. 2014).

We obtained an NIR spectrum of SN 2021zby on 2021 September 25 using the SpeX spectrograph (Rayner et al. 2003) on the NASA InfraRed Telescope Facility (IRTF). We used the low-resolution prism mode with the $0''.8$ slit, providing a resolving power of $R \sim 75$ with a simultaneous coverage between 0.7 and 2.5 μm . We observed an A0V star HIP16095

immediately after the SN for telluric correction and flux calibration. We reduced the data using `spectool` (Cushing et al. 2004), which performed flat-field correction, wavelength calibration, and spectral extraction. Telluric correction was performed using `xtellcor` (Vacca et al. 2003). The optical and NIR spectral series of SN 2021zby are shown in Figure 2.

3. Analysis

3.1. Fitting Light Curve with Models

There are a number of semianalytical shock-cooling light-curve models available, including Piro (2015, hereafter **P15**), Piro et al. (2021, hereafter **P21**), and Sapir & Waxman (2017, hereafter **SW17**). **P15** is the simplest of these, making no assumption about the density profile of the progenitor and assuming a simple expanding photosphere. **P21** is a revision of the **P15** model, which improves upon **P15** by employing a two-component velocity model. **P21** model the progenitor with outer material, which has a steep velocity gradient, and inner material with a shallow velocity gradient. **SW17** assume the progenitor has a polytropic density profile. This is characterized by the polytropic index n that is equal to $3/2$ for progenitors with a convective envelope, such as red supergiants (RSGs) or yellow supergiants (YSGs), and is equal to 3 for progenitors with a radiative envelope, such as blue supergiants (BSGs). Each model is parameterized by envelope mass (M_e), envelope radius (R_e), ejecta velocity (v), and start time (t), which is relative to the peak of the radioactive portion of the light curve.

Each of these models assume that the progenitor radiates as a blackbody and uses an analytical description of the luminosity, radius, and temperature of the progenitor over time in order to derive the flux of the shock-cooling light curve. Full details of these analytical models can be found in Armstrong et al. (2021), who we closely follow.

Following Armstrong et al. (2021), we fit the shock-cooling models using an affine-invariant Markov Chain Monte Carlo method (`ShockCooling.jl`³⁸). This algorithm produces an approximate posterior for a model, given data, priors, and a likelihood function. Our data consist of the ATLAS-*o* and the 6 hr binned TESS light curve, up to ~ 7 days after explosion, the time when the shock-cooling light curve transitions into the radioactive light curve. Our likelihood function is chosen to be the reduced χ^2 between the models and our data. Both bands are fitted simultaneously, and the combined reduced χ^2 is then minimized. The reduced χ^2 , defined as χ^2 divided by the degrees of freedom of each band, allows us to weight each reduced χ^2 by the number of data points, accounting for the larger sample of TESS data. Due to the degeneracy inherent in the models, the models are very sensitive to choice of prior. As such, we used an iterative approach to defining the priors, starting with large uniform priors with $0 < R_e/R_\odot < 5000$ and $0 < M_e/M_\odot < 5000$, and then shrunk the prior until the posterior contained the complete 95% contour, without the prior extending too far from the 95% contour. The prior of ejecta velocity is constrained to be $12500 \pm 800 \text{ km s}^{-1}$, determined by the FWHM of the 1.1 μm feature around the shock-cooling peak as discussed in the following section. Our final priors for each parameter are listed in Table 1. The best-fit values of **SW17** models satisfy the validity range of temperature $T > 0.7 \text{ eV}$ within the fitting range.

³³ Note that this estimation can be biased because the optical and NIR spectra only cover the Rayleigh–Jeans tail and thus may not reflect the true temperature of photosphere.

³⁴ <https://github.com/svalenti/pessto>

³⁵ The pipeline is publicly accessible at https://github.com/msiebert1/UCSC_spectral_pipeline.

³⁶ https://github.com/LCOGT/floyds_pipeline

³⁷ <https://www.mso.anu.edu.au/pywifef/doku.php>

³⁸ <https://github.com/OmegaLambda1998/ShockCooling>

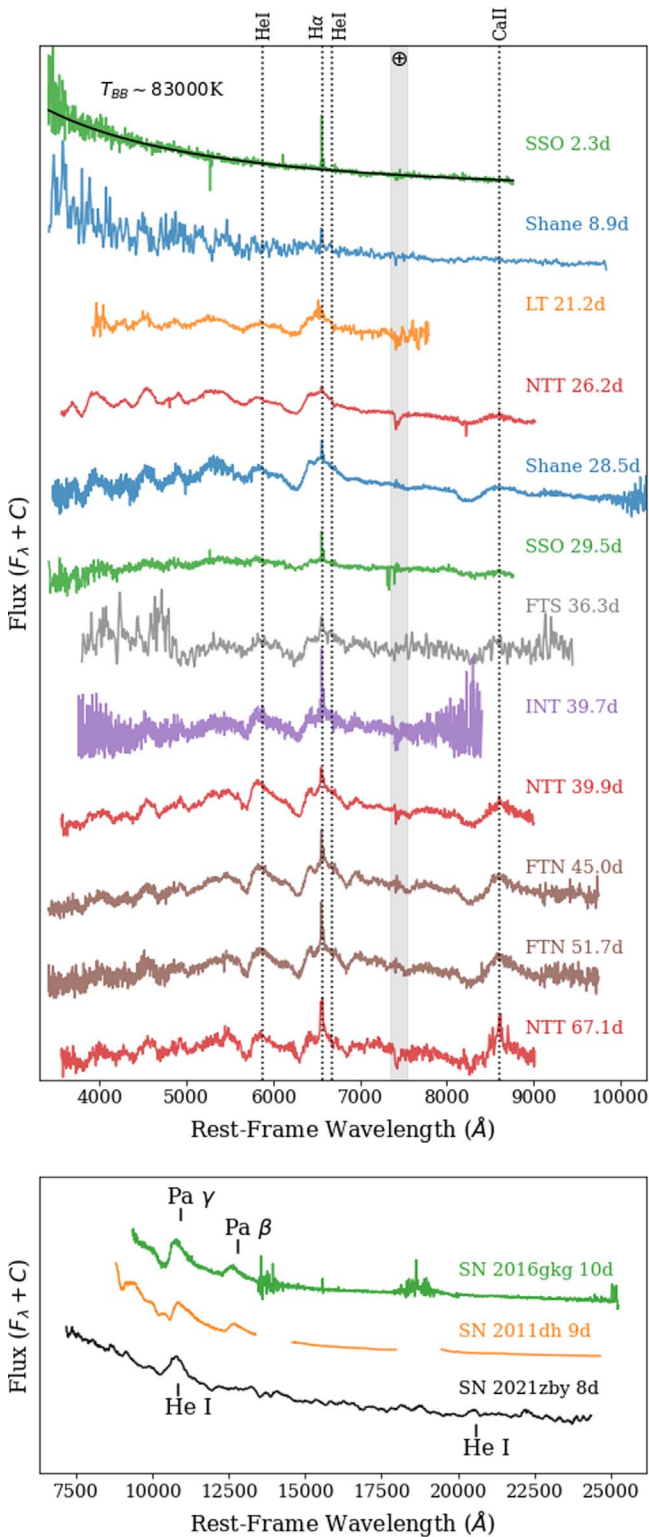


Figure 2. Top: optical spectral series of SN 2021zby with phases and telescopes labeled above. Spectra taken with different telescopes are plotted with different colors. Bottom: NIR spectrum of SN 2021zby taken by IRTF around the shock-cooling peak, in comparison with SN 2011dh (Ergon et al. 2015) and SN 2016gkg (Tartaglia et al. 2017) around a similar phase. The phases relative to the peak and relevant lines are labeled on the spectra. The telluric line in between 7170 and 7350 Å in the observer frame has been marked as the gray region. All the spectra have been normalized and shifted vertically for display purposes.

(The data used to create this figure are available.)

The fitting results for four models discussed are also included in Table 1 and plotted in Figure 3. Figure 4 shows the corner plots of posterior distributions of each parameter. This plot shows the marginalized maximum likelihood, the 68% isolikelihood levels of the marginalized maximum likelihood, as well as the total maximum-likelihood point in the four-dimensional parameter space. Among these models, SW17 $n = 3/2$ models have significantly smaller residuals and larger log-likelihood than the other models. Additionally, although the P15 and P21 models are able to fit the light curve, they have significant systematic changes in their residuals. Thus, from the light-curve fit alone, the SW17 $n = 3/2$ models are preferable in general. This is also reflected in the maximum-likelihood points of the P15 and P21 models, both of which have $R_e > 1500R_\odot$, the upper limit of stellar radius according to current stellar evolution theories (Levesque et al. 2005). Constraining the fit to smaller radii produces a much poorer quality fit that cannot constrain the rise of the SCL. Note that the one-dimensional posterior is the integration of the four-dimensional posterior and unavoidably lost information, so the marginal maximum-likelihood point can deviate from the maximum-likelihood point, but they still agree with each other within the uncertainty range in general.

3.2. Spectroscopic Features

As shown in Figure 2, the optical spectra around the shock-cooling phase are dominated by blackbody continuum with $T_{BB} \gtrsim 10^4$ K with few line features except the narrow H α emission from the host. In Figure 5, we further include the optical spectra from other SNe Iib with SCL around the shock-cooling phase and the late phase. Around the shock-cooling peak, there is no detection of broad H α emission in the spectra of SN 2021zby, which is a prominent feature in SN 2011dh and SN 2016gkg at a similar phase (Arcavi et al. 2011; Tartaglia et al. 2017). Benetti et al. (1994) reported the discovery of narrow lines with $v < 1000$ km s $^{-1}$ in SN 1993J around the shock-cooling phase, including H α , He II, [Fe X], and [Fe XIV], and claimed that those narrow emission lines are signals of circumstellar medium (CSM) interaction. Such features are not seen in the early spectra of SN 2021zby, possibly due to the relatively low S/N and spectral resolution. As shown in Figures 2 and 5, the optical spectra after the shock-cooling phase during the radioactive peak start to resemble the spectral evolution of a typical SN Iib.

The weak H α feature of SN 2021zby is persistent and still observable even at 43 days after the radioactive peak. This is different from SN 1993J for which the H α feature significantly weakened at a similar phase (Matheson et al. 2000). This may indicate a sizeable mass of hydrogen in the progenitor of SN 2021zby.

The NIR spectrum taken by IRTF around the shock-cooling peak is plotted in the bottom panel of Figure 2 in comparison with NIR spectra of SN 2016gkg and SN 2011dh around a similar phase. The only significant feature is the broad emission line at around 10800 Å, which may come from Pa γ , He I 1.083 μ m, C I 1.0693 μ m, or Mg II 1.0927 μ m as discussed in Shahbandeh et al. (2022). Unlike SN 2011dh and SN 2016gkg, there is no detection of a Pa β 1.2818 μ m feature. On the other hand, a weak emission feature is present around He I 2.0581 μ m, while there are no detections of Mg II 2.1369 μ m in the NIR or any other H I or C I features in the optical

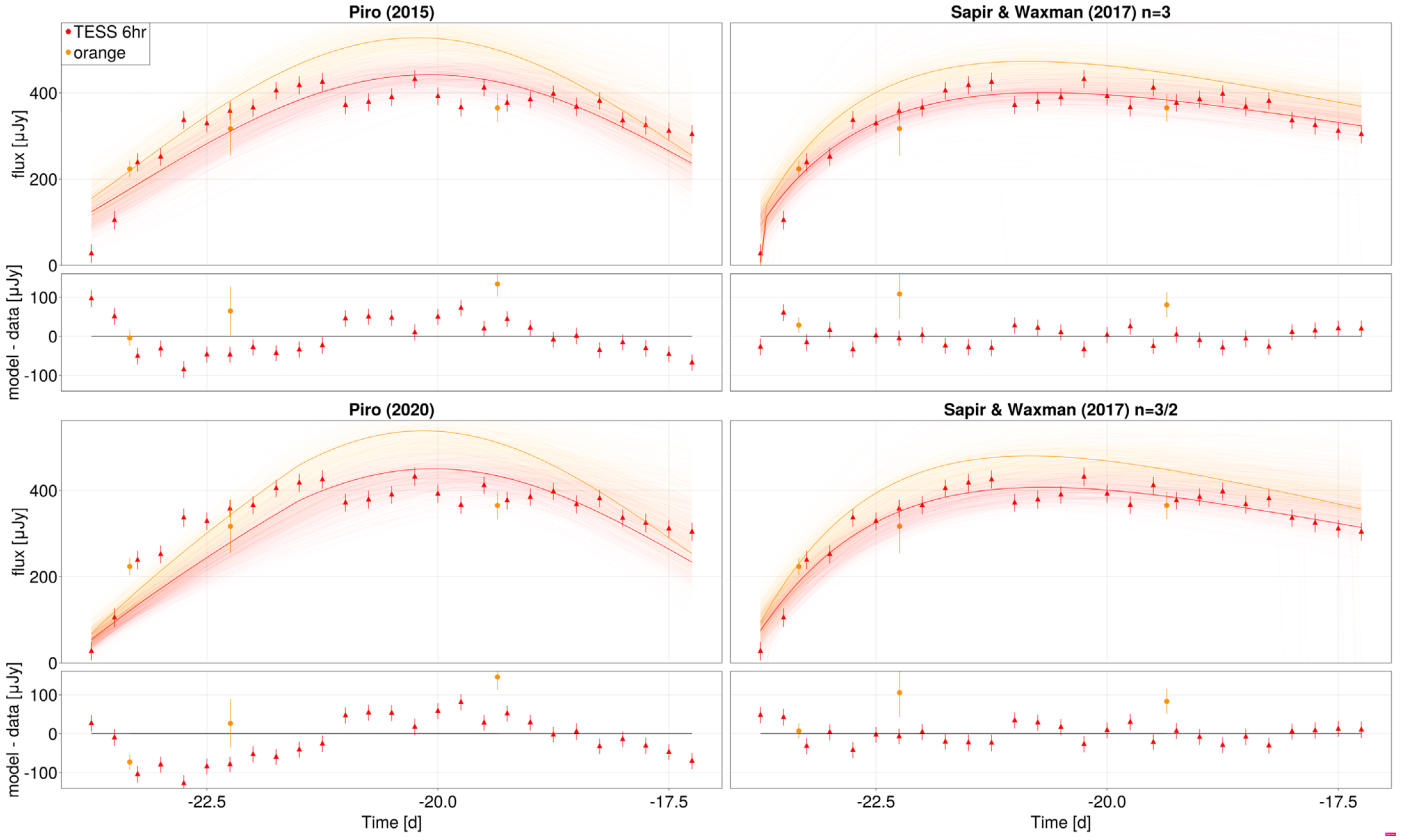


Figure 3. Model fits for the TESS and ATLAS-*o* light curve of SN 201zby during the shock-cooling phase. Solid lines show the maximum-likelihood best fit, while transparent lines are 500 randomly sampled parameters, which are indicative of the spread in the posterior. Time is relative to inferred TESS maximum.

Table 1
Priors and Results of Shock-cooling Models fit to the Shock-cooling Light Curve of SN 201zby

Parameter	$M_e (M_\odot)$	$R_e (R_\odot)$	v (km s $^{-1}$)	t (days)	Log-likelihood
SW17 $n = 3/2$ Prior	Uniform [0, 2]	Uniform [0, 500]	Normal 12500 ± 800	Normal -24 ± 0.1	...
SW17 $n = 3/2$ Marginal Max Likelihood	$0.31^{+0.34}_{-0.092}$	$127.51^{+166.37}_{-9.80}$	$12499.48^{+716.63}_{-816.28}$	$-24.00^{+0.081}_{-0.098}$	-14.00
SW17 $n = 3/2$ Max Likelihood	0.258	430.80	12514.33	-23.98	...
SW17 $n = 3$ Prior	Uniform [0, 10]	Uniform [0, 750]	Normal 12500 ± 800	Normal -24 ± 0.1	...
SW17 $n = 3$ Marginal Max Likelihood	$2.45^{+2.54}_{-0.44}$	$125.02^{+328.35}_{-8.25}$	$12350^{+817.60}_{-697.91}$	$-24.00^{+0.096}_{-0.082}$	-16.04
SW17 $n = 3$ Max Likelihood	2.18	732.53	12404.25	-23.98	...
P15 Prior	Uniform [0, 0.15]	Uniform [0, 2500]	Normal 12500 ± 800	Normal -24 ± 0.1	...
P15 Marginal Max Likelihood	$0.061^{+0.009}_{-0.005}$	$1524.99^{+328.35}_{-312.75}$	$12250.06^{+751.97}_{-710.78}$	$-24.015^{+0.099}_{-0.089}$	-15.14
P15 Max Likelihood	0.062	1633.45	12230.0	-24.01	...
P21 Prior	Uniform [0, 0.25]	Uniform [0, 5000]	Normal 12500 ± 800	Normal -24 ± 0.1	...
P21 Marginal Max Likelihood	$0.073^{+0.026}_{-0.012}$	$2625^{+1390.10}_{-1190.10}$	$12749.78^{+641.47}_{-721.56}$	$-24.045^{+0.083}_{-0.102}$	-18.19
P21 Max Likelihood	0.069	3988.67	12605.93	-24.068	...

Note. The analytical models used are highly degenerate so are very sensitive to choice of prior. Each model was initially given a large M_e and R_e prior (0–5000 in each respective unit). These priors were then iteratively shrunk until the M_e and R_e posteriors were complete, i.e., the 95% contours were not cut off, nor did the prior extend far beyond the 95% contour. The v prior was chosen from constraints calculated via a Gaussian fit to He I 10830 Å around the shock-cooling peak. Finally the constraint on t was chosen from the position of the first TESS observation. We include both the maximum-likelihood point without uncertainty, and the one-dimensional, marginalized maximum likelihood with uncertainty. We calculate the uncertainty by finding the 68% isolikelihood levels. The log-likelihood of each model fit is also listed.

spectrum at a similar phase. We therefore conclude that this $1.1 \mu\text{m}$ feature most likely comes from He I $1.083 \mu\text{m}$. We measure the FWHM of this $1.1 \mu\text{m}$ feature with a simple Gaussian fit and use it as the prior of the ejecta velocity in the light-curve fitting (see Table 1).

4. Discussion and Conclusion

The progenitor of SN 201zby is likely to have a moderately extended envelope to produce a clear shock-cooling peak, but not as extended as those of SN IIP progenitors as the peak is not blended with the radioactive peak. With the high-cadence

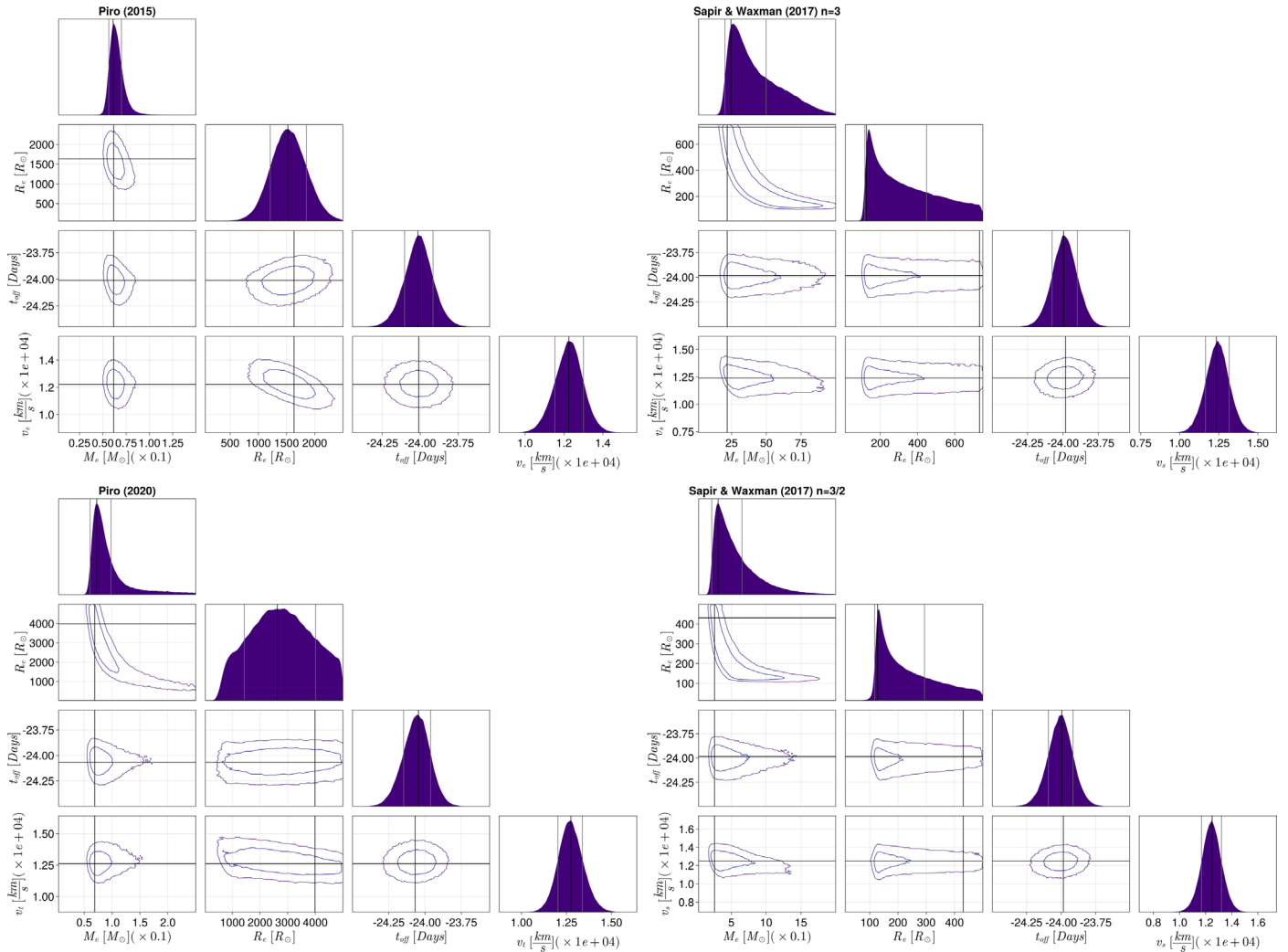


Figure 4. Corner plots of our light-curve fit to SN 2021zby. The blue contours show the 68% probability density contour, and the purple contours show the 95% probability density contour. The solid black line in the contour plots show the point of maximum likelihood, while the marginalized histograms show the maximum marginalized likelihood, as well as the 68% isolikelihood levels. Note that since we have four parameters, our contour plots are also marginalized so the maximum-likelihood point is not guaranteed to agree with the 2D maximum likelihood.

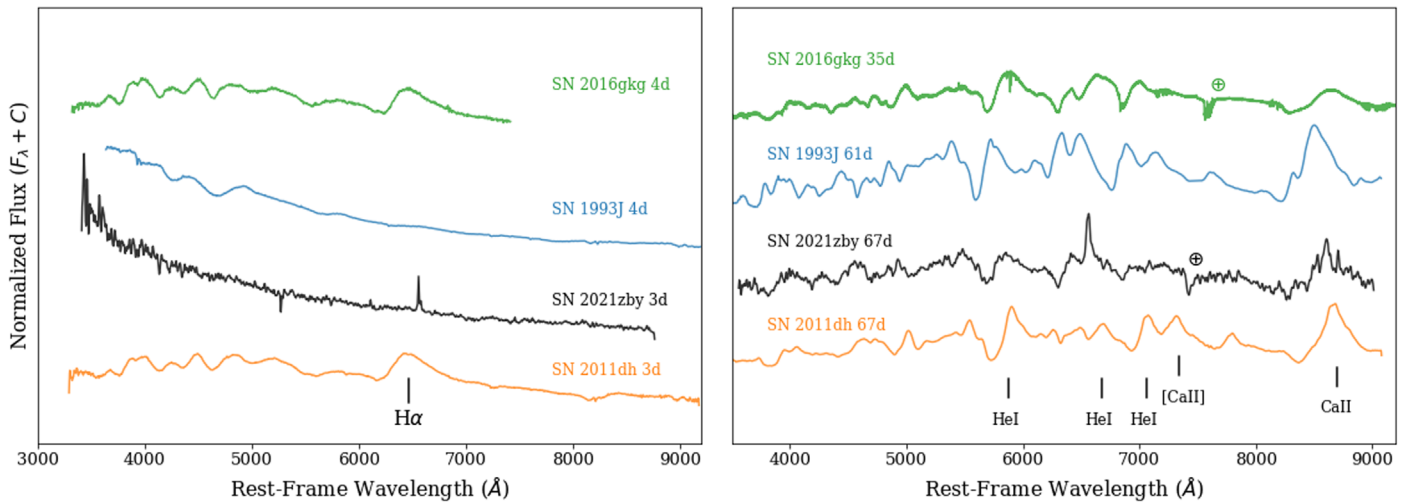


Figure 5. The spectra of SN 2021zby on 3 days (left) and 67 days (right) after explosion, in comparison with SN 2016gkg (Tartaglia et al. 2017), SN 2011dh (Ergon et al. 2015), and SN 1993J (Matheson et al. 2000). All the spectra have been normalized and shifted for clarity.

TESS and ATLAS *—o* light curves covering the full shock-cooling phase of SN 2021zby, we are able to constrain the progenitor’s properties with relatively high precision compared to ground-based observations alone. We fit the multiband light curves following the fitting scheme described in Armstrong et al. (2021), and the results are summarized as below:

1. The SW17 $n = 3/2$ model (convective envelope, i.e., similar to those of RSGs or YSGs) is the best fit among the four models, indicating a progenitor with an envelope mass of $\sim 0.30\text{--}0.65 M_{\odot}$ and an envelope radius of $\sim 120\text{--}300 R_{\odot}$.
2. The $n = 3$ (radiative envelope, i.e., similar to that of BSG) models have relatively larger log-likelihood and indicate an envelope mass of $\sim 2.0\text{--}5.0 M_{\odot}$ and an envelope radius of $\sim 120\text{--}450 R_{\odot}$. However, such an envelope radius is significantly larger than the expected radii of BSGs, which are in the range of $40\text{--}80 R_{\odot}$ (Underhill et al. 1979). This implies that it is physically inconsistent with observations of the structure of BSGs.
3. The P15 and P21 models have similar performance as SW17 $n = 3$ model, though they fail to fully reproduce the rapid rise. They are less preferable as both models indicate a progenitor radius of $R_e \gtrsim 1500 R_{\odot}$, the upper limit of stellar radius according to current stellar evolution theories.

In the previous study on SN 2017jgh, a similar fitting schemes was applied to its Kepler light curve (Armstrong et al. 2021), and they also found that the SW17 $n = 3/2$ model is the best-fit model, while the SW17 $n = 3$ model performs marginally worse. The best-fit result of SN 2017jgh indicates its progenitor to be most likely a YSG with an envelope radius $R_e \sim 50\text{--}290 R_{\odot}$ and an envelope mass $M_e \lesssim 1.7 M_{\odot}$. A few other SNe I Ib have progenitors discovered in pre-SN images, enabling another approach to constrain progenitor properties. Aldering et al. (1994) identify the progenitor of SN 1993J as a YSG of type K0 Ia with SED and luminosity and estimated the radius to be $\sim 500 R_{\odot}$. For SN 2016gkg, Kilpatrick et al. (2022) constrained the progenitor to be a YSG as well, with radius $\sim 70 R_{\odot}$, which matches the $40\text{--}150 R_{\odot}$ estimate from the light-curve fit by Arcavi et al. (2017a). For SN 2011dh, Bersten et al. (2012) compared its g light curve with models and also found a YSG with $R \sim 200 R_{\odot}$ to be the best match for its progenitor, which is confirmed by the pre- and postexplosion images (Van Dyk et al. 2013). The progenitor radius of SN 2021zby estimated from the best-fit SW17 $n = 3/2$ model lies in between these SNe I Ib confirmed with YSG progenitors, indicating that SN 2021zby may have a YSG progenitor as well, though the possibility of an RSG progenitor cannot be excluded by current light-curve fitting alone.

The early spectra of SN 2021zby during SCL show clear differences compared to the other SNe I Ib with similar SCLs. Unlike SN 2011dh and SN 2016gkg, SN 2021zby lacks H features in the shock-cooling phase. Such a phenomenon might be a consequence of high ionization around the shock-cooling phase (Dessart et al. 2018). This argument is further supported by the blue continuum of the early spectra. On the other hand, the presence of broad He I10830 at early times and a relatively strong H α feature after 43 days postpeak indicates that the progenitor still had a sizable amount of H and He.

The high cadences of Kepler and TESS are crucial to sufficiently constrain the progenitor properties with the model

fitting of the SCL. However, even with such exquisite data, it is still challenging to fully break the degeneracy between the RSG and YSG progenitors, which could be distinguished either through observations in the UV band, where the signal is most prominent, or by constraining the wind speed with the flash ionized features with high-resolution spectra. Improving modeling on the spectroscopic evolution will be another key to breaking the degeneracy. With improving cadence and receiving earlier alerts from, for example, Rubin Observatory (Ivezić et al. 2019) in the near future, we can expect to have better time and wavelength coverage in bluer bands. In the longer term, the next generation of MIDEX space-based UV telescopes, e.g., UVEX (Kulkarni et al. 2021) and STAR-X (Saha et al. 2017), will allow us to monitor SCLs in the UV.

The author acknowledges Luc Dessart, Eli Waxman, Nir Sapor, Ryosuke Hirai., and Sasha Kozyreva for the valuable discussion.

This Letter includes data collected by the TESS mission. Funding for the TESS mission is provided by the NASA’s Science Mission Directorate. The TESS data presented in this paper were obtained from the Mikulski Archive for Space Telescopes (MAST) at the Space Telescope Science Institute (STScI). The specific observations analyzed can be accessed via doi:10.17909/0cp4-2j79. STScI is operated by the Association of Universities for Research in Astronomy, Inc., under NASA contract NAS5-26555. Support to MAST for these data is provided by the NASA Office of Space Science via grant NAG5-7584 and by other grants and contracts.

This work makes use of data from Las Cumbres Observatory. The LCO group is supported by NSF grants AST-1911225 and AST-1911151.

This work was funded by ANID, Millennium Science Initiative, ICN12_009.

The Isaac Newton Telescope is operated on the island of La Palma by the Isaac Newton Group of Telescopes in the Spanish Observatorio del Roque de los Muchachos of the Instituto de Astrofísica de Canarias (I/2021B/14).

This work is partially based on observations collected at the European Organisation for Astronomical Research in the Southern Hemisphere, Chile, as part of ePESSTO+ (the advanced Public ESO Spectroscopic Survey for Transient Objects Survey). ePESSTO+ observations were obtained under ESO program IDs 1103.D-0328, 106.216C, 108.220C (PI: Inserra).

Q.W. is supported in part by NASA grants 80NSSC22K0494, 80NSSC21K0242, and 80NSSC19K0112.

I.A. is a CIFAR Azrieli Global Scholar in the Gravity and the Extreme Universe Program and acknowledges support from that program, from the European Research Council (ERC) under the European Union’s Horizon 2020 research and innovation program (grant agreement number 852097), from the Israel Science Foundation (grant number 2752/19), from the United States—Israel Binational Science Foundation (BSF), and from the Israeli Council for Higher Education Alon Fellowship.

The UCSC team is supported in part by NASA grant 80NSSC20K0953, NSF grant AST-1815935, the Gordon & Betty Moore Foundation, the Heising-Simons Foundation, and by a fellowship from the David and Lucile Packard Foundation to R.J.F.

L.G. and T.E.M.B. acknowledge financial support from the Spanish Ministerio de Ciencia e Innovación (MCIN), and the Agencia Estatal de Investigación (AEI) 10.13039/501100011033 under the PID2020-115253GA-I00 HOST-FLOWS project, from Centro Superior de Investigaciones Científicas (CSIC) under the PIE project 20215AT016 and the I-LINK 2021 LINKA20409, and the program Unidad de Excelencia María de Maeztu CEX2020-001058-M. L.G. additionally acknowledges the European Social Fund (ESF) “Investing in your future” under the 2019 Ramón y Cajal program RYC2019-027683-I.

M.G. is supported by the European Union’s Horizon 2020 research and innovation program under grant agreement No. 101004719.

N.I. was partially supported by Polish NCN DAINA grant No. 2017/27/L/ST9/03221.

J.D.L. and D.O.N. acknowledge support from a UK Research and Innovation Fellowship (MR/T020784/1).

M.N. is supported by the European Research Council (ERC) under the European Union’s Horizon 2020 research and

innovation program (grant agreement No. 948381) and by a Fellowship from the Alan Turing Institute.

S.J.S., S.S., D.R.Y., and K.W.S. acknowledge funding from STFC grants ST/T000198/1 and ST/S006109/1.

Facilities: TESS, Shane, NTT, FTN, FTS, IRTF, DECam, ATLAS, INT, SSO:2.3 m, LT.

Software: astropy (Astropy Collaboration et al. 2013, 2018), TESSreduce (Ridden-Harper et al. 2021), ShockCooling.jl (<https://github.com/OmegaLambda1998/ShockCooling>), Matplotlib (Hunter 2007), SciPy (Virtanen et al. 2020), NumPy (Harris et al. 2020), pysynphot (STScI Development Team 2013).



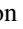
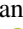

Appendix

A log of the spectroscopic observations is provided in Table 2.

Table 2
Log of Spectroscopic Observations of SN 2021zby

MJD	Phase Relative to t_0 (days)	Phase Relative to t_{peak} (days)	Telescope/Instrument	Wavelength Range (Å)
59,476.745	2.29	−21.69	SSO 2.3 m/WiFeS	3500–9000
59,482.491	7.89	−16.09	IRTF/SpeX	6848–25,378
59,483.466	8.84	−15.14	Shane/KAST	3506–10094
59,496.114	21.16	−2.81	LT/SPRAT	4020–7994
59,501.265	26.18	2.21	NTT/EFOSC2	3652–9248
59,503.594	28.45	4.48	Shane/KAST	3256–10,896
59,504.653	29.48	5.51	SSO 2.3 m/WiFeS	3500–9000
59,511.619	36.28	12.30	FTS/FLOYDS	3500–10,000
59,515.092	39.66	15.68	INT/IDS	3855–8627
59,515.300	39.86	15.89	NTT/EFOSC2	3651–9245
59,520.520	44.95	20.98	FTN/FLOYDS	3500–10,000
59,527.470	51.73	27.75	FTN/FLOYDS	3500–10,000
59,543.206	67.06	43.08	NTT/EFOSC2	3652–9248

ORCID iDs

Qinan Wang  <https://orcid.org/0000-0001-5233-6989>
 Patrick Armstrong  <https://orcid.org/0000-0003-1997-3649>
 Yossef Zenati  <https://orcid.org/0000-0002-0632-8897>
 Ryan Ridden-Harper  <https://orcid.org/0000-0003-1724-2885>
 Armin Rest  <https://orcid.org/0000-0002-4410-5387>
 Iair Arcavi  <https://orcid.org/0000-0001-7090-4898>
 Charles D. Kilpatrick  <https://orcid.org/0000-0002-5740-7747>
 Ryan J. Foley  <https://orcid.org/0000-0002-2445-5275>
 Brad E. Tucker  <https://orcid.org/0000-0002-4283-5159>
 Chris Lidman  <https://orcid.org/0000-0003-1731-0497>
 Thomas L. Killestein  <https://orcid.org/0000-0002-0440-9597>
 Melissa Shahbandeh  <https://orcid.org/0000-0002-9301-5302>
 Joseph P Anderson  <https://orcid.org/0000-0003-0227-3451>
 Chris Ashall  <https://orcid.org/0000-0002-5221-7557>
 Jamison Burke  <https://orcid.org/0000-0003-0035-6659>
 Ting-Wan Chen  <https://orcid.org/0000-0002-1066-6098>
 Kyle A. Dalrymple  <https://orcid.org/0000-0001-8737-9700>
 Kyle W. Davis  <https://orcid.org/0000-0002-5680-4660>
 Michael D. Fulton  <https://orcid.org/0000-0003-1916-0664>
 Lluís Galbany  <https://orcid.org/0000-0002-1296-6887>
 Estefania Padilla Gonzalez  <https://orcid.org/0000-0003-0209-9246>
 Bore Gao  <https://orcid.org/0000-0002-9902-6803>
 Mariusz Gromadzki  <https://orcid.org/0000-0002-1650-1518>
 D. Andrew Howell  <https://orcid.org/0000-0003-4253-656X>
 Jacob E. Jencson  <https://orcid.org/0000-0001-5754-4007>
 David O. Jones  <https://orcid.org/0000-0002-6230-0151>
 Joseph D. Lyman  <https://orcid.org/0000-0002-3464-0642>
 Curtis McCully  <https://orcid.org/0000-0001-5807-7893>
 Tomás E. Müller-Bravo  <https://orcid.org/0000-0003-3939-7167>
 Megan Newsome  <https://orcid.org/0000-0001-9570-0584>
 Matt Nicholl  <https://orcid.org/0000-0002-2555-3192>
 Craig Pellegrino  <https://orcid.org/0000-0002-7472-1279>
 Sofia Rest  <https://orcid.org/0000-0002-3825-0553>
 Stephen J. Smartt  <https://orcid.org/0000-0002-8229-1731>
 Ken Smith  <https://orcid.org/0000-0001-9535-3199>
 Shubham Srivastav  <https://orcid.org/0000-0003-4524-6883>
 Giacomo Terreran  <https://orcid.org/0000-0003-0794-5982>
 Samaporn Tinyanont  <https://orcid.org/0000-0002-1481-4676>
 David R. Young  <https://orcid.org/0000-0002-1229-2499>
 Alfredo Zenteno  <https://orcid.org/0000-0001-6455-9135>

References

- Alard, C., & Lupton, R. H. 1998, *ApJ*, 503, 325
 Aldering, G., Humphreys, R. M., & Richmond, M. 1994, *AJ*, 107, 662
 Andrews, J. E., Pearson, J., Lundquist, M. J., et al. 2022, *ApJ*, 938, 19
 Arcavi, I., Gal-Yam, A., Yaron, O., et al. 2011, *ApJL*, 742, L18
 Arcavi, I., Hosseinzadeh, G., Brown, P. J., et al. 2017a, *ApJL*, 837, L2
 Arcavi, I., Howell, D. A., Kasen, D., et al. 2017b, *Natur*, 551, 210
 Armstrong, P., Tucker, B. E., Rest, A., et al. 2021, *MNRAS*, 507, 3125
 Arnett, W. D., & Meakin, C. 2011, *ApJ*, 741, 33
 Arnett, W. D., Hirschi, R., Campbell, S. W., et al. 2018, arXiv:1810.04659
 Astropy Collaboration, Price-Whelan, A. M., Sipőcz, B. M., et al. 2018, *AJ*, 156, 123
 Astropy Collaboration, Robitaille, T. P., Tollerud, E. J., et al. 2013, *A&A*, 558, A33
 Becker, A. 2015, HOTPANTS: High Order Transform of PSF ANd Template Subtraction, Astrophysics Source Code Library, ascl:1504.004
 Benetti, S., Patat, F., Turatto, M., et al. 1994, *A&A*, 285, L13
 Bersten, M. C., Benvenuto, O. G., Nomoto, K., et al. 2012, *ApJ*, 757, 31
 Bertin, E., Mellier, Y., Radovich, M., et al. 2002, in ASP Conf. Ser. 281, *Astronomical Data Analysis Software and Systems XI*, ed. D. A. Bohlender, D. Durand, & T. H. Handley (San Francisco, CA: ASP), 228
 Berton, M., Congiu, E., Benetti, S., & Yaron, O. 2018, *TNSCR*, 2018-1726, 1
 Buzzoni, B., Delabre, B., Dekker, H., et al. 1984, *Msngr*, 38, 9
 Cao, Y., Kasliwal, M. M., Arcavi, I., et al. 2013, *ApJL*, 775, L7
 Chen, Z. H., Yan, L., Kangas, T., et al. 2022, arXiv:2202.02060
 Childress, M. J., Vogt, F. P. A., Nielsen, J., & Sharp, R. G. 2014, *Ap&SS*, 349, 617
 Clocchiatti, A., Wheeler, J. C., Brotherton, M. S., et al. 1996, *ApJ*, 462, 462
 Cushing, M. C., Vacca, W. D., & Rayner, J. T. 2004, *PASP*, 116, 362
 DePoy, D., Abbott, T., Annis, J., et al. 2008, *Proc. SPIE*, 7014, 70140E
 Dessart, L., Hillier, D. J., Livne, E., et al. 2011, *MNRAS*, 414, 2985
 Dessart, L., Hillier, D. J., Sukhbold, T., Woosley, S. E., & Janka, H. T. 2021, *A&A*, 656, A61
 Dessart, L., Yoon, S.-C., Livne, E., & Waldman, R. 2018, *A&A*, 612, A61
 Dimitriadis, G., Foley, R. J., Rest, A., et al. 2019, *ApJL*, 870, L1
 Dopita, M., Hart, J., McGregor, P., et al. 2007, *Ap&SS*, 310, 255
 Drout, M. R., Soderberg, A. M., Gal-Yam, A., et al. 2011, *ApJ*, 741, 97
 Ensmann, L. M., & Woosley, S. E. 1988, *ApJ*, 333, 754
 Ergon, M., Jerkstrand, A., Sollerman, J., et al. 2015, *A&A*, 580, A142
 Fang, Q., Maeda, K., Kuncarayakti, H., et al. 2022, *ApJ*, 928, 151
 Fausnaugh, M., Vallely, P., Kochanek, C., et al. 2021, *ApJ*, 908, 51
 Filippenko, A. V., Matheson, T., & Ho, L. C. 1993, *ApJL*, 415, L103
 Filippenko, A. V., & Sargent, W. L. W. 1985, *Natur*, 316, 407
 Flaughner, B., Diehl, H. T., Honscheid, K., et al. 2015, *AJ*, 150, 150
 Flewelling, H. A., Magnier, E. A., Chambers, K. C., et al. 2020, *ApJS*, 251, 7
 Folatelli, G., Bersten, M. C., Benvenuto, O. G., et al. 2014, *ApJL*, 793, L22
 Foley, R. J., Smith, N., Ganeshalingam, M., et al. 2007, *ApJL*, 657, L105
 Fulton, M., Smartt, S. J., Sim, S. A., et al. 2021, *TNSCR*, 2021-3521, 1
 Gagliano, R., Post, R., Weinberg, E., Newton, J., & Puckett, T. 2018, *TNSTR*, 2018-1685, 1
 Gal-Yam, A. 2017, in *Handbook of Supernovae*, ed. A. W. Alsabti & P. Murdin (Cham: Springer), 195
 Gilkis, A., & Arcavi, I. 2022, *MNRAS*, 511, 691
 Gilkis, A., Vink, J. S., Eldridge, J. J., & Tout, C. A. 2019, *MNRAS*, 486, 4451
 Gomez, S., Berger, E., Hosseinzadeh, G., et al. 2021, *ApJ*, 913, 143
 Haas, M. R., Batalha, N. M., Bryson, S. T., et al. 2010, *ApJL*, 713, L115
 Harris, C. R., Millman, K. J., van der Walt, S. J., et al. 2020, *Natur*, 585, 357
 Heger, A., Fryer, C. L., Woosley, S. E., Langer, N., & Hartmann, D. H. 2003, *ApJ*, 591, 288
 Hinkle, J. 2021, *TNSCR*, 2021-3283, 1
 Howell, S. B., Sobeck, C., Haas, M., et al. 2014, *PASP*, 126, 398
 Huber, M., Chambers, K. C., Flewelling, H., et al. 2015, *ATel*, 7153, 1
 Hunter, J. D. 2007, *CSE*, 9, 90
 Ivezić, Ž., Kahn, S. M., Tyson, J. A., et al. 2019, *ApJ*, 873, 111
 Jacobson-Galán, W. V., Dessart, L., Jones, D. O., et al. 2022, *ApJ*, 924, 15
 Karamehmetoglu, E., Sollerman, J., Taddia, F., et al. 2022, arXiv:2210.09402
 Kilpatrick, C. D., Coulter, D. A., Foley, R. J., et al. 2022, *ApJ*, 936, 111
 Kilpatrick, C. D., Drout, M. R., Auchettl, K., et al. 2021, *MNRAS*, 504, 2073
 Kulkarni, S. R., Harrison, F. A., Grefenstette, B. W., et al. 2021, arXiv:2111.15608
 Levesque, E. M., Massey, P., Olsen, K. A. G., et al. 2005, *ApJ*, 628, 973
 Lohev, N., Sabach, E., Gilkis, A., & Soker, N. 2019, *MNRAS*, 490, 9
 Long, G., Song, H.-F., Zhang, R.-Y., et al. 2022, *RAA*, 22, 055016
 Matheson, T., Filippenko, A. V., Barth, A. J., et al. 2000, *AJ*, 120, 1487
 Maund, J. R., Fraser, M., Ergon, M., et al. 2011, *ApJL*, 739, L37
 Maund, J. R., Smartt, S. J., Kudritzki, R. P., Podsiadlowski, P., & Gilmore, G. F. 2004, *Natur*, 427, 129
 Nakar, E., & Sari, R. 2010, *ApJ*, 725, 904
 Pearson, J., Hosseinzadeh, G., Sand, D. J., et al. 2022, arXiv:2208.14455
 Piascik, A. S., Steele, I. A., Bates, S. D., et al. 2014, *Proc. SPIE*, 9147, 91478H
 Piro, A. L. 2015, *ApJL*, 808, L51 (P15)
 Piro, A. L., Haynie, A., & Yao, Y. 2021, *ApJ*, 909, 209 (P21)
 Prentice, S. J., Mazzali, P. A., Pian, E., et al. 2016, *MNRAS*, 458, 2973
 Rayner, J. T., Toomey, D. W., Onaka, P. M., et al. 2003, *PASP*, 115, 362
 Rest, A., Scolnic, D., Foley, R. J., et al. 2014, *ApJ*, 795, 44
 Rest, A., Stubbs, C., Becker, A. C., et al. 2005, *ApJ*, 634, 1103
 Ricker, G. R., Winn, J. N., Vanderspek, R., et al. 2014, *Proc. SPIE*, 9143, 914320

- Ridden-Harper, R., Rest, A., Hounsell, R., et al. 2021, arXiv:2111.15006
- Riess, A. G., Casertano, S., Yuan, W., et al. 2018, *ApJ*, **861**, 126
- Riess, A. G., Macri, L. M., Hoffmann, S. L., et al. 2016, *ApJ*, **826**, 56
- Saha, T. T., Zhang, W. W., & McClelland, R. S. 2017, *Proc. SPIE*, **10399**, 103990I
- Sana, H., de Mink, S. E., de Koter, A., et al. 2012, *Sci*, **337**, 444
- Sapir, N., & Waxman, E. 2017, *ApJ*, **838**, 130 (SW17)
- Schechter, P. L., Mateo, M., & Saha, A. 1993, *PASP*, **105**, 1342
- Schlafly, E. F., & Finkbeiner, D. P. 2011, *ApJ*, **737**, 103
- Scolnic, D., Casertano, S., Riess, A., et al. 2015, *ApJ*, **815**, 117
- Shahbandeh, M., Hsiao, E. Y., Ashall, C., et al. 2022, *ApJ*, **925**, 175
- Smartt, S. J., Valenti, S., Fraser, M., et al. 2015, *A&A*, **579**, A40
- Smith, K. W., Smartt, S. J., Young, D. R., et al. 2020, *PASP*, **132**, 085002
- Smith, K. W., Srivastav, S., Smartt, S. J., et al. 2021, *TNSAN*, **246**, 1
- Smith, N. 2017, in *Handbook of Supernovae*, ed. A. W. Alsabti & P. Murdin (Cham: Springer), 403
- Smith, N., Foley, R. J., & Filippenko, A. V. 2008, *ApJ*, **680**, 568
- Soker, N. 2017, *MNRAS*, **470**, L102
- Springob, C. M., Haynes, M. P., Giovanelli, R., & Kent, B. R. 2005, *ApJS*, **160**, 149
- Sravan, N., Marchant, P., Kalogera, V., Milisavljevic, D., & Margutti, R. 2020, *ApJ*, **903**, 70
- STScI Development Team 2013, pynsphot: Synthetic photometry software package, Astrophysics Source Code Library, ascl:1303.023
- Tartaglia, L., Fraser, M., Sand, D. J., et al. 2017, *ApJL*, **836**, L12
- Tody, D. 1986, *Proc. SPIE*, **627**, 733
- Tonry, J., Denneau, L., Heinze, A., et al. 2018, *PASP*, **130**, 064505
- Underhill, A. B., Divan, L., Prevot-Burnichon, M. L., & Doazan, V. 1979, *MNRAS*, **189**, 601
- Vacca, W. D., Cushing, M. C., & Rayner, J. T. 2003, *PASP*, **115**, 389
- Valdes, F., Gruendl, R. & DES Project 2014, in *ASP Conf. Ser.* 485, *Astronomical Data Analysis Software and Systems XXIII*, ed. N. Manset & P. Forshay (San Francisco, CA: ASP), 379
- Valenti, S., Sand, D., Pastorello, A., et al. 2013, *MNRAS*, **438**, L101
- Vallely, P. J., Fausnaugh, M., Jha, S. W., et al. 2019, *MNRAS*, **487**, 2372
- Van Dyk, S. D., Zheng, W., Clubb, K. I., et al. 2013, *ApJL*, **772**, L32
- Van Dyk, S. D., Zheng, W., Fox, O. D., et al. 2014, *AJ*, **147**, 37
- Virtanen, P., Gommers, R., Oliphant, T. E., et al. 2020, *NatMe*, **17**, 261
- Wang, Q., Rest, A., Zenati, Y., et al. 2021, *ApJ*, **923**, 167
- Woosley, S. E., Heger, A., & Weaver, T. A. 2002, *RvMP*, **74**, 1015
- Woosley, S. E., Langer, N., & Weaver, T. A. 1993, *ApJ*, **411**, 823
- Yaron, O., & Gal-Yam, A. 2012, *PASP*, **124**, 668
- Yoon, S.-C., Dessart, L., & Clocchiatti, A. 2017, *ApJ*, **840**, 10
- Zenati, Y., Wang, Q., Bobrick, A., et al. 2022, arXiv:2207.07146